Full-core nuclear fuel simulation of boron free SMR: potential fuel safety challenges of i-SMR

Chansoo Lee [a], Kyuseok Shim [a], Hyuntaek Rho [a], Jooil Yoon [b], Youho Lee [a*]
[a]*Department of Nuclear Eng., Seoul National Univ., 1 Gwanak-ro, Gwanak-gu, Seoul 08826, Republic of Korea*
[b]*KEPCO International Nuclear Graduate School, Ulsan, Republic of Korea*
**Corresponding author: leeyouho@snu.ac.kr*

Keywords: boron free SMR, core simulation, 2D fuel simulation, pellet cladding interaction.

1. Introduction

Various types of Small Modular Reactors (SMR) are being proposed to meet energy demands. Korea is developing the i-SMR (innovative-SMR), which is based on the pressurized water reactor (PWR) type SMR. It features boron-free operation and an integrated reactor design.

In PWRs, typically three methods are used to control excess reactivity: control rods, burnable poisons, and boric acid. Without boric acid, additional burnable poisons or manipulation of control rods are needed to reduce excess reactivity. Increasing burnable poison rods adds additional power burden on the other fuel rods. Also, operation of control rods alters local power distribution when withdrawn during reactor operation.

Additionally, the small core size of SMRs leads to increased neutron leakage which makes local power difference increase. Also, i-SMR adopts 2-batch refueling strategy which relatively increases reactivity swing compared to 3-batch loading pattern [1]. As a result, i-SMR have to control larger excess reactivity, while experiencing more significant power fluctuations compared to conventional PWRs.

These power variants changes fuel pellet and cladding temperature, which induce thermal expansion. As thermal expansion of pellet is more significant than cladding in terms of both thermal expansion coefficient and temperature [2], pellet cladding interaction (PCI) behavior could be significant in SMR operation.

Therefore, this study conducted full-core nuclear fuel analyses comparing boron-free SMR to conventional PWRs based on 3D power distribution results from reactor core calculations. The fuel simulation results were compared to assess the impact of boron-free operation on SMR nuclear fuel.

2. Simulation condition

To determine the total core power, a core analysis was conducted using the 2D(planar)/1D(axial) pin-by-pin neutron diffusion code, SPHINCS [3]. Following the reconstruction of the power history for each fuel rod, a safety analysis was performed using the nuclear fuel simulation code, GIFT [4]. GIFT adopts 2D (r, z) structural analysis model, which is applicable to pellet cladding mechanical interaction (PCMI) analysis, and hydrogen model including hydrogen reorientation and diffusion [5, 6].

2.1. Simulation condition

Detailed conditions of SMR and PWR core and fuel are listed in table I. figure 1, and 2 shows the SMR's CEDM configuration and fuel assembly types of equilibrium cycle. The SMR and PWR consist of 69 and 177 fuel assemblies, respectively, and use 2-batch and 3-batch loading patterns. For the nuclear fuel simulation, pin-by-pin data were reorganized into 9 groups for the SMR and 13 groups for the PWR. A total of 5,300 fuel rods were analyzed.

Table I: i-SMR and PWR specification

Features	Value	
	i-SMR [7]	PWR
Thermal power [MW]	520	2815
Cycle length [EFPD]	753	388
Cycle burnup [MWD/MTU]	20,000	14,000
Number of batch	2	3
Number of fuel assembly	69	177
U-235 enrichment [%]	4.95	3.6
Assembly type	17x17	16x16
Active fuel length [cm]	240	381
Burnable poison	UO_2-Gd_2O_3, Gd_2O_3-Al_2O_3 (HIGA)	UO_2-Gd_2O_3
Plenum length [cm]	25.4	25.4
Cladding type	PRXA	CWSR
Coolant mass flux [kg/m^{2}s]	2030	3567

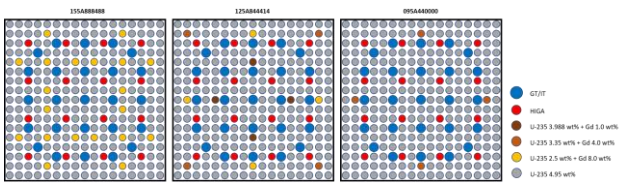

Fig. 1. Cross-section of equilibrium cycle's fuel assembly types

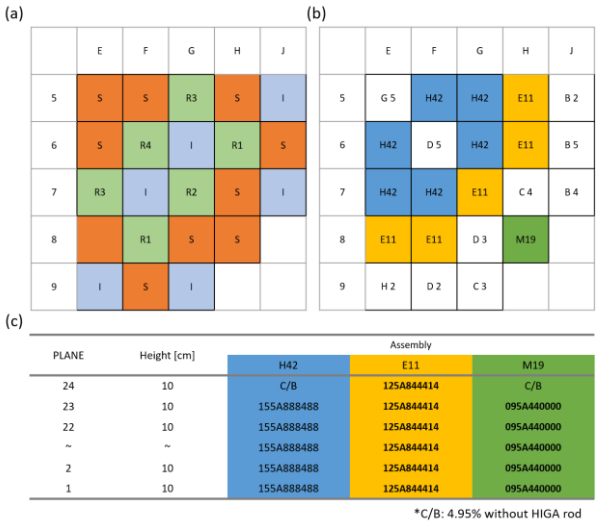

PLANE	Height [cm]	Assembly H42	Assembly E11	Assembly M19
24	10	C/B	125A844414	C/B
23	10	155A888488	125A844414	095A440000
22	10	155A888488	125A844414	095A440000
~	~	155A888488	125A844414	095A440000
2	10	155A888488	125A844414	095A440000
1	10	155A888488	125A844414	095A440000

Fig. 2. Quarter core configuration (a) CEDM arrangement, S: shutdown bank, R: regulating control rod bank, I: In-Core Instrument Assembly, (b) refueling pattern, (c) axial profile of equilibrium cycle's fuel assemblies

3. Simulation result and discussion

3.1 Core simulation result

Based on table I. figure 1, and 2, SMR and PWR core are calculated and results are illustrated in figure 3, 4, and 5. Figure 3 shows the axial shape index (ASI) and peaking factor, Fq and Fxy.

The peaking factor was higher in the SMR because of low-leakage loading pattern, where once burnt assemblies are placed at the core periphery, and due to the smaller core size. The ASI and its fluctuation range were also larger in the SMR, which are because of the control rod operation.

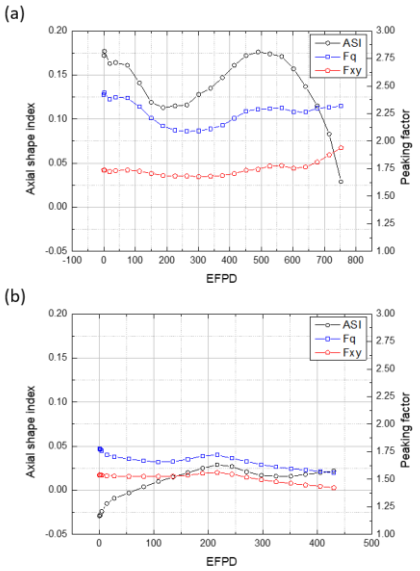

Fig. 3. Axial shape index, peaking factors of (a) SMR and (b) PWR

Figure 4(a) and (b) shows the reactivity control method, which is control rod position for SMR and critical boron concentration for PWR. In the SMR, the initial position of control rods results in higher power in the lower half of the core, leading to a higher ASI. As operation continues and reactivity decreases, the R3 and R4 banks are gradually withdrawn, as shown in figure 4(a), increasing the power in the upper region of the core and causing the ASI to decrease. On the other hand, in a PWR, ASI does not significantly changes during operation because the boron concentration in the coolant is adjusted for reactivity control.

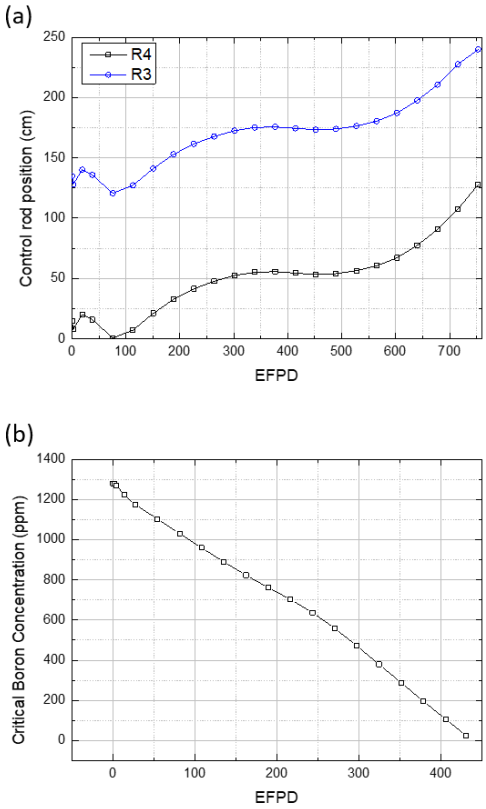

Fig. 4. Reactivity control (a) SMR: control rod operation, (b) PWR: critical boron concentration

Figure 5(a) and (b) shows the core averaged axial power distribution at the beginning of xenon equilibrium, middle and end of cycle. As anticipated from the ASI and R3, R4 bank positions in figure 3(a) and 4(a), the axial power in the upper region increased. In contrast, in the case of the PWR, only a slight power reduction is observed due to the decrease in fissile in the core center.

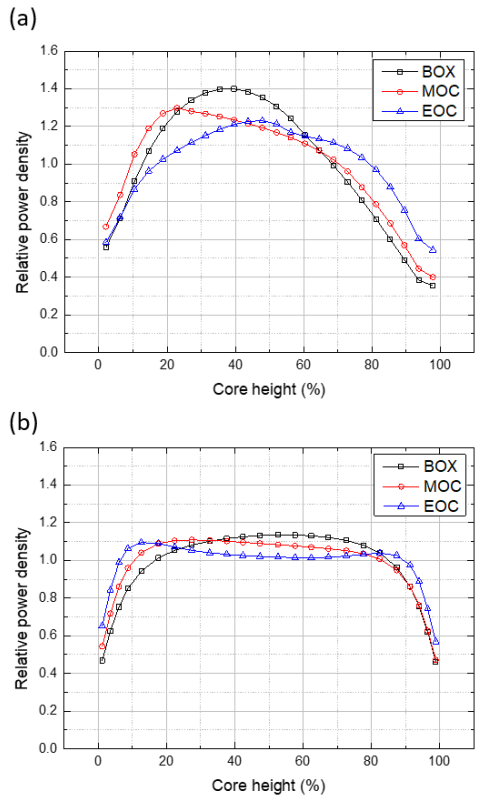

Fig. 5. Core averaged axial power distributions at the beginning of xenon equilibrium, middle, and end of cycle (a) SMR, (b) PWR

Figure 6(a) and (b) show the axial pin power distribution for the fuel rod with the most significant axial power variation. Figure 6(a) shows that the local power variant at the mid-height of the assembly where the R4 bank is located is approximately 1.2, which is equivalent to power change of 13 kW/m over the cycle. In contrast, the power variation in the PWR is at most 0.3, with a change of only around 5 kW/m during cycle.

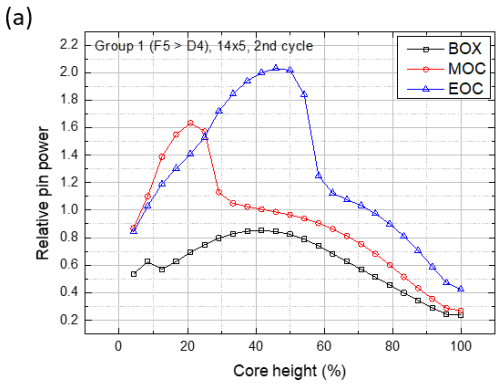

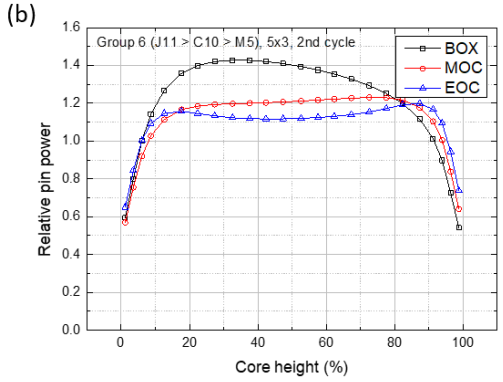

Fig. 6. Axial power distribution of the pin where the axial power distribution of the fuel rod changes the most at the beginning of xenon equilibrium, middle, and end of cycle (a) SMR, (b) PWR

3.2 Fuel simulation result

3.2.1 Severe case

Based on the core simulation result, pin power histories were rebuilt as input, and the specific node power histories are shown in figure 7(a) and (b). Figure 7(a) shows 2 cases, which are rapid power increase (Case 1: Group 1, 14x5) and power jump after refueling (Case 2: Group 8, 14x5).

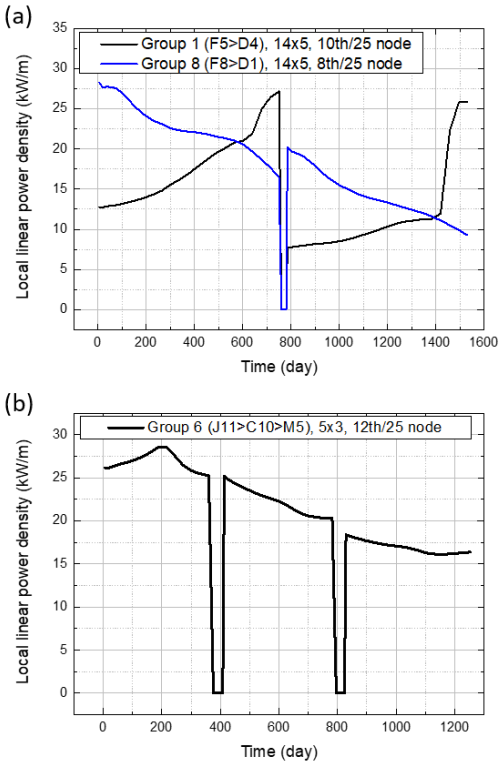

Fig. 7. Local axial pin power history of (a) SMR – rapid power increase and power jump, (b) PWR

Figure 8 shows the mechanical gap throughout operation. Mechanical gap decreases over time due to creep as a function of the time spent in the core, and it also decreases with increasing power due to thermal expansion from the rise in pellet temperature (see 650 to 750 days in Figure 8(a): case 1). Comparing the results of the two cases, in case 1, the lower power level prevented the gap from closing during the first cycle. However, in case 2, the higher power caused the mechanical gap to close during the first cycle. In the PWR, the gap remains open during the first and second cycles but closes during at the beginning of third cycle.

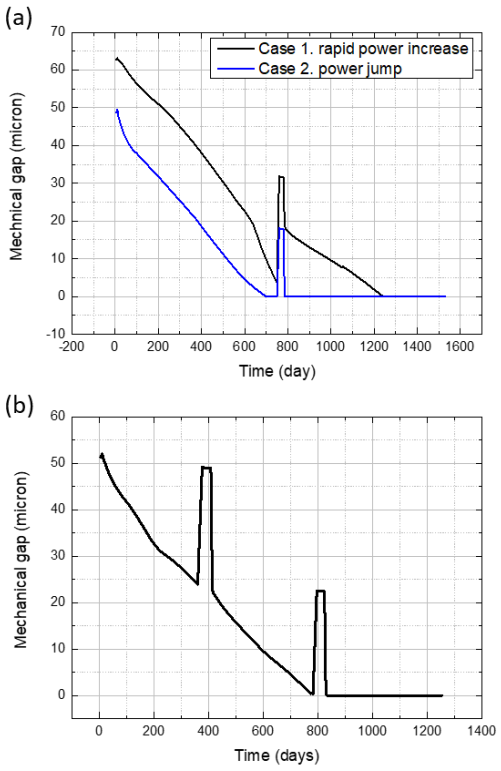

Fig. 8. Mechanical gap of (a) SMR – rapid power increase and power jump, (b) PWR

Figure 9 shows cladding hoop stress of SMR and PWR. Case 1 of figure 9(a) shows extremely high hoop stress at the end of second cycle, which is due to the power increasement after PCMI (see figure 7(a) and 8(a)). Manipulation of control rod due to boron-free operation causes significant local power variations, which increase the pellet temperature and fission gas release in the affected zone. The cladding that experiences PCMI is subjected to tensile stress from the pellet. When power increases, thermal expansion and swelling intensify this tensile stress.

Case 2 of figure 9(a) shows relatively high hoop stress, which is due to a power jump after refueling. During overhaul, thermal expansion causes the pellet-cladding gap to reopen. Then, the fuel is then subjected to a higher power level than before, the strain in the pellet exceeds the previous cladding strain, resulting in significant tensile stress on the cladding.

Figure 9(b) shows hoop stress in PWR. Before the gap closure, compressive stress induces cladding to creep down, while pellet swells. After PCMI, pellet swelling causes an increase in tensile stress on the cladding, as burnup increases.

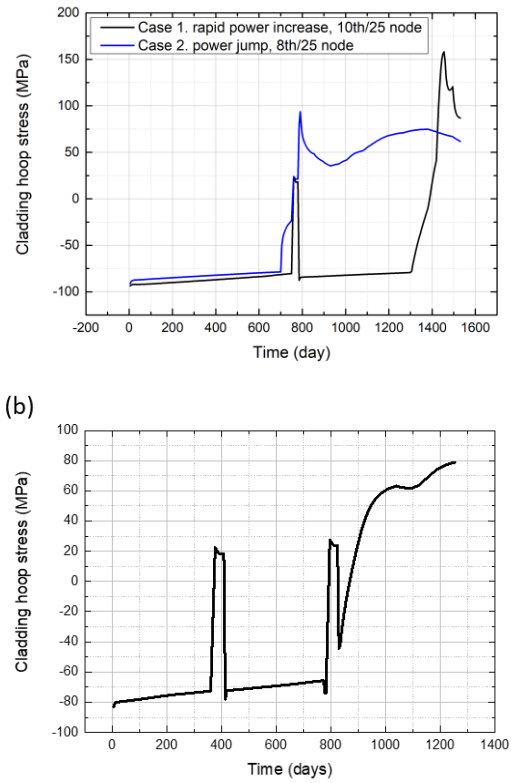

Fig. 9. Cladding hoop stress of (a) SMR – rapid power increase and power jump, (b) PWR

Fuel simulation results show two mechanisms of hoop stress increment. The first mechanism is tensile stress resulting from pellet swelling following PCMI, which is due to burnup increase. This mechanism always occurs in both PWR and SMR as burnup increases during reactor operation.

The second is tensile stress caused by thermal expansion due to a power increase after PCMI. This mechanism occurred only in SMR, and it can be divided into two reasons. The first reason is that once burnt assemblies are moved to regulating control rod bank positions (Case 1: Rapid power increase, which is refueled to R4). The second is when the assembly that experienced PCMI in the first cycle is reloaded in a direction that increases power (Case 2: Power jump).

3.2.2 Full core analysis

Figure 10 shows histogram of fuel analysis of SMR (9 groups, 2232 fuel rods) and PWR (13 groups, 3068

fuel rods): hoop stress, hoop strain, oxide thickness, hydrogen concentration, radial hydride fraction (RHF), and rod averaged burnup. The results except for rod averaged burnup are nodal maximum value.

Hoop stress of PWR reaches a maximum of 80 MPa, whereas in an SMR, maximum hoop stress reaches up to 180 MPa due to the operation of the control rods. Hoop stress histogram indicates that SMR experiences unexpected hoop stress level, which can increase threat of stress corrosion cracking and delayed hydride cracking. Another point is that SMR shows the wide hoop stress distribution. Due to the smaller core size, power distribution of SMR is less uniform compared to a PWR, resulting in a broader hoop stress distribution.

For the same reason, the cladding hoop strain in the SMR also shows a broader distribution. The core averaged maximum cladding hoop strain is greater in PWR. Hoop strain can be divided into elastic deformation due to pressure load, thermal strain, plastic deformation due to creep, and deformation caused by pellet swelling after PCMI. Since the system pressure and cladding design are similar, the elastic deformation due to pressure load and thermal strain have minimal difference.

In case of deformation caused by creep and pellet swelling after mechanical gap closure, SMR uses PRXA cladding which has larger creep rate compared to CWSR cladding. Therefore, SMR experience more inward creep deformation before PCMI. As a result, the most frequent value of SMR is around -0.5%, indicating that the cladding has deformed inward more significantly compared to a PWR.

After PCMI, the cladding is pushed outward due to pellet. In SMR, both radial and axial peaking factors are larger compared to those in a PWR, resulting in higher nodal burnup. Consequently, some fuel rods experience greater deformation due to pellet swelling, leading to increased cladding hoop strain.

The oxide layer thickness and hydrogen concentration are significantly lower in SMRs, mainly because the thermal-hydraulic design values of the two reactors are similar, but SMRs use PRXA cladding that has had Sn removed, which is more resistant to corrosion. On the other hand, RHF increases by up to 8% in SMRs.

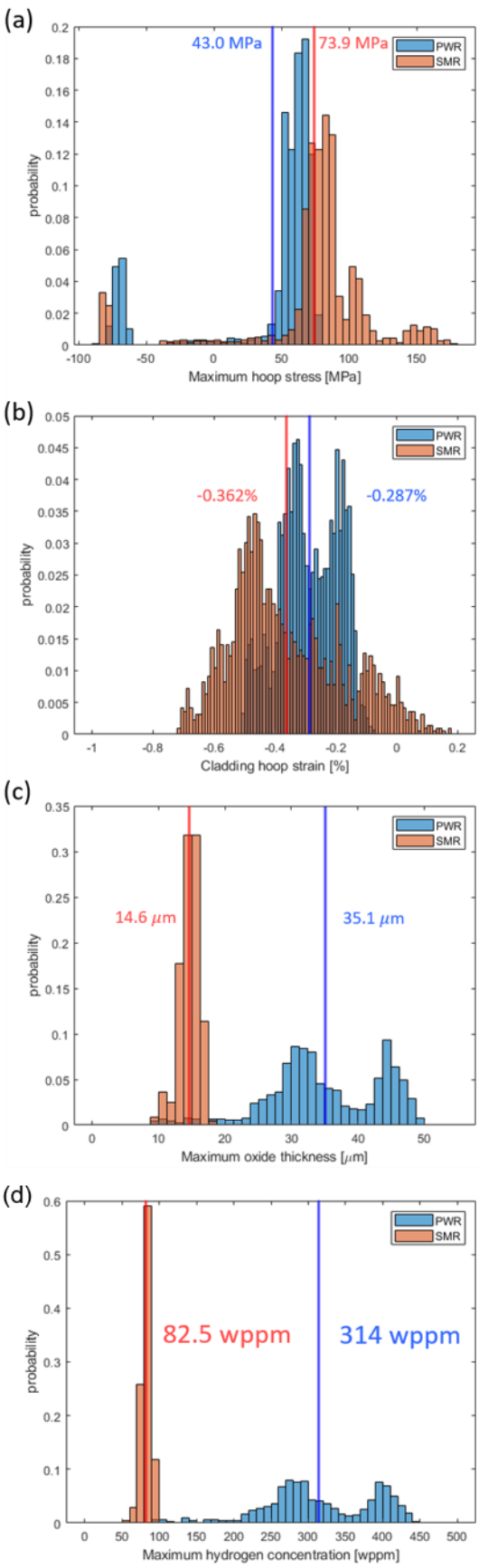

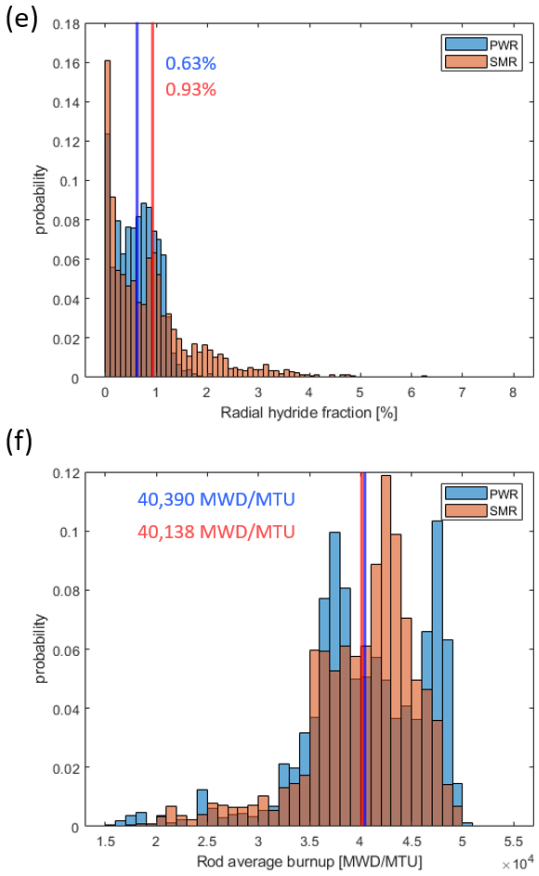

Fig. 10. Histogram of full core fuel analysis of SMR and PWR. (a) Maximum cladding hoop stress, (b) Maximum cladding hoop strain, (c) Maximum cladding oxide thickness, (d) Maximum hydrogen concentration, (e) Maximum radial hydride fraction, (f) rod averaged burnup. Blue and red line stand for average value.

4. Conclusion

In this study, full-core SMR and PWR fuel analyses were conducted based on the core calculation. Boron free operation affected on the local power variation, which increases hoop stress due to PCMI. Additionally, two batch refueling enlarges local power difference. When nuclear fuel that has previously experienced PCMI is refueled into the higher power location, the hoop stress can increase.

To enhance nuclear fuel safety, two approaches can be taken in core design. First, avoid placing once-burnt operated. Second, minimize the power increase of nuclear fuel that has experienced PCMI by applying a low-leakage loading pattern.

From a fuel design standpoint, adopting PRXA cladding to maximize ductility and corrosion resistance is one option, while another is alleviating PCMI to increase thermal conductivity and reduce thermal expansion by using doped pellets.

Nevertheless, the above approaches are limited to 5% enrichment and do not consider load-following operation. With the future demand of LEU+ for burnup increase and load following operation, a potential safety challenges are expected due to the lack of boric acid.

ACKNOWLEDGEMENT

This work was supported by the National Research Foundation of Korea (NRF) grant funded by the Ministry of Science and ICT (MSIT) of the Republic of Korea [No. RS-2024-00420956]. This work was supported by the Institute of Engineering Research at Seoul National University.

REFERENCES

[1] M. J. Driscoll, T. J. Downar, and E. E. Pilat, *The linear reactivity model for nuclear fuel management*. American nuclear society, 1990.

[2] W. G. Luscher and K. J. Geelhood, "Material property correlations: comparisons between FRAPCON-3.4, FRAPTRAN 1.4, and MATPRO," Pacific Northwest National Lab.(PNNL), Richland, WA (United States), 2010.

[3] H. Hong and J. Yoon, "Solution of OECD/NEA PWR MOX/UO2 benchmark with a high-performance pin-by-pin core calculation code," *Nuclear Engineering and Technology*, 2024.

[4] K. Sim and Y. Lee, "Fuel Performance Code for Light Water Reactor, GIFT: Current development status and path-forward," presented at the Transactions of the Korean Nuclear Society Spring Meeting, Jeju, Republic of Korea, May 18-19, 2023, 2023. [Online]. Available: https://www.kns.org/files/pre_paper/49/23S-503-%EC%8B%AC%EA%B7%9C%EC%84%9D.pdf.

[5] C. Lee and Y. Lee, "Simulation of hydrogen diffusion along the axial direction in zirconium cladding tube during dry storage," *Journal of Nuclear Materials*, vol. 579, p. 154352, 2023.

[6] C. Jo and Y. Lee, "Development of Advanced Hydride Reorientation Model and Experimental Validation " presented at the Korean nuclear society spring meeting, Jeju, Korea, 2024. [Online]. Available: https://www.kns.org/files/pre_paper/51/24S-314-%EC%A1%B0%EC%B0%BD%ED%98%84.pdf.

[7] J. S. Kim, T. S. Jung, and J. Yoon, "Reactor core design with practical gadolinia burnable absorbers for soluble boron-free operation in the innovative SMR," *Nuclear Engineering and Technology*, 2024.